



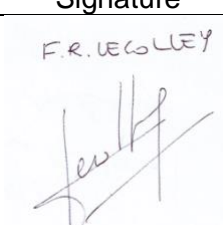
**HORIZON 2020**

# HORIZON 2020 RESEARCH AND INNOVATION FRAMEWORK PROGRAMME OF THE EUROPEAN ATOMIC ENERGY COMMUNITY

## **Nuclear Fission and Radiation Protection 2018 (NFRP-2018-4)**

Project acronym: **SANDA**  
Project full title: **Solving Challenges in Nuclear Data for the Safety of European Nuclear facilities**  
Grant Agreement no.: **H2020 Grant Agreement number: 847552**

Workpackage N°: **WP2**  
Identification N°: **D2.2**  
Type of document: **Deliverable**  
Title: Report on the (n,chp) cross section measurements  
Dissemination Level: **PU**  
Reference:  
Status: **VERSION 1**  
Comments:

|                  | Name            | Partner | Date       | Signature   |
|------------------|-----------------|---------|------------|---|
| Prepared by:     | F.R. Lecolley   | 5       | 02/07/2024 | <br>F.R. LECOLEY |
| WP leader:       | Daniel Cano-Ott | 1       |            |   |
| IP Co-ordinator: | E. González     | 1       |            |   |



## I. Study of (n, $\alpha$ ) reactions of interest for nuclear reactors: the SCALP Project

A. Chevalier<sup>1,\*</sup>, F.-R. Lecolley<sup>1</sup>, G. Lehaut<sup>1</sup>, J.-L. Lecouey<sup>1</sup>, N Marie<sup>1</sup>, L Manduci<sup>2</sup>, X Ledoux<sup>3</sup>, R. Beyer<sup>4</sup>, A. Junghans<sup>4</sup>, O. Bouland<sup>5</sup>, and O. Serot<sup>5</sup>

1 LPC Caen, 6 Bd Maréchal Juin, Caen 14000, France

2 EAMEA, BP 19 50115, Cherbourg Armées 50100, France

3 GANIL, Bd Henri Becquerel, Caen 14000, France

4 HZDR, Bautzner Landstrasse 400, Dresden 01328, Germany

5 CEA, DES, IRESNE Cadarache, Saint-Paul-lez-Durance 13108, France

### Introduction

The (n, $\alpha$ ) cross-sections on oxygen 16 and fluorine 19 are of great interest for the improvement and/or development of the nuclear reactors. Significant differences have been observed for those nuclei regarding the (n, $\alpha$ ) channel:

- On oxygen 16, discrepancies up to 30% between experimental data and/or evaluation are observed and are responsible for an uncertainty of 100 pcm on the  $k_{\text{eff}}$  or reactor using either water and/or oxide fuel [1].
- On fluorine 19, discrepancies up to a factor 3 between experimental data and/or evaluation are observed (Fig.1). Estimated uncertainty on the total neutron interaction cross-section of  $^{19}\text{F}$  bring up to 213 pcm uncertainty on the reactor  $k_{\text{eff}}$  value. The uncertainty on the cross-section of the reaction  $^{19}\text{F}(n,\alpha)^{16}\text{N}$  alone is responsible for approximately 40 pcm to 130 pcm of uncertainty on  $k_{\text{eff}}$  depending on the type of MSR considered.[2]

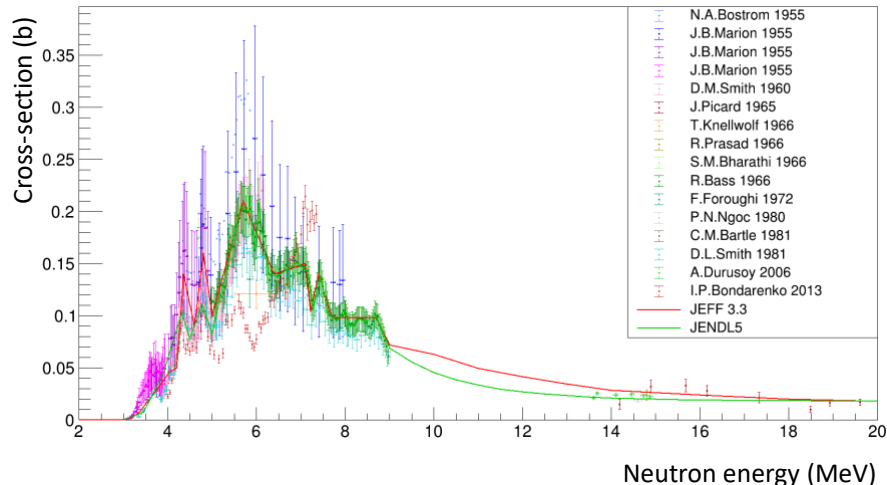


Figure 1 –  $^{19}\text{F}(n,\alpha)^{16}\text{N}$  cross-section extracted from the EXFOR library (NEA/OCDE)

In view of improving our knowledge on this (n, $\alpha$ ) reactions, the GrACE group (Groupe Aval du Cycle Electronucléaire) of the LPC Caen has developed a new detector named SCALP (Scintillating ionization Chamber for ALPha particle detection in neutron induced reactions). This report deals with the first experiment carried out with this brand-new detector at the new NFS facility (GANIL, Caen, France).

### 1 - Experimental setup

For this new measurement, the GrACE group at LPC Caen has developed a new detector called SCALP. SCALP is an ionization chamber filled with a scintillation gas, which allows

reaction detections with a good time resolution, making the device particularly suited to neutron time-of-flight based measurements.

### The SCALP detector

The SCALP detector is a closed pressure vessel. Fig.1 shows that four photomultipliers (PMTs) are positioned around the chamber to detect photons coming from scintillation due to the interaction of charged particles produced by neutron-induced reactions with the CF<sub>4</sub> gas. This gas was chosen for its scintillation properties to optimize measurement resolution in addition to containing the fluorine target. The time resolution of the PMTs was measured to be 250 ps ( $1\sigma$ ) using an alpha source [3], which allows one to reconstruct the neutron time of flight with a very good resolution. On the other hand, the ionization chamber enclosed in the vessel was able to measure the energy deposited by charged particles with a resolution of 170 keV ( $1\sigma$ ).

The SCALP detector can also be filled with a gas mixture made of CF<sub>4</sub> (97%) and CO<sub>2</sub> (3%) in order to measure (n, $\alpha$ ) reactions on oxygen 16. Addition of CO<sub>2</sub> has an impact on the performances of the detector with a degradation of the time and energy resolutions respectively to 770 ps ( $1\sigma$ ).and 250 keV ( $1\sigma$ ).

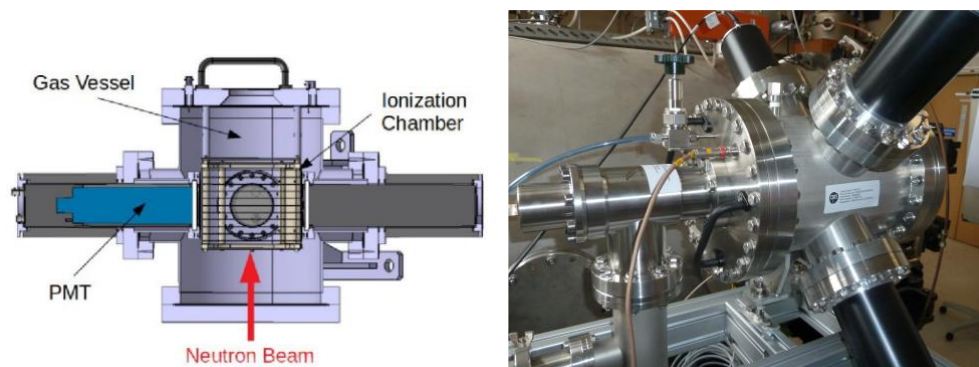


Figure 2. SCALP detector schematic [3] (left) and a photo of the SCALP detector (right). It includes a gas vessel containing the ionization and scintillation gas plus the target gas and 4 photomultipliers for measuring the time of flight of incident neutrons. The ionization chamber measures the energy deposited by the charged reaction products.

### The NFS (Neutron For Science) facility at SPIRAL2 (GANIL, Caen, France)

SPIRAL2 is a superconducting linear accelerator from GANIL (LINAG) in Caen, France. It accelerates a beam of light ions (p, d, 4He) using accelerator cavities, with a beam intensity of up to 5 mA for deuterons at the frequency of 88 MHz. A chopper can be used in order to decrease this frequency, it can select 1/100 to 1/1000 of the charged particle bursts.

NFS is an experimental area (Fig.3) where neutrons can be produced from a primary deuteron beam and a beryllium target. These neutrons then pass through a first collimator in order to get a well define neutron beam with a spot radius of 2.6 cm before entering the 30m time-of-flight (TOF) area, where various types of detectors can be set up. In addition, a second collimator can be installed in the TOF area in order to get a beam spot with a limited radius at the end of the area. The neutron beam supplied is a continuous energy spectrum ranging from 0.1 to 40 MeV peaked at 14 MeV.

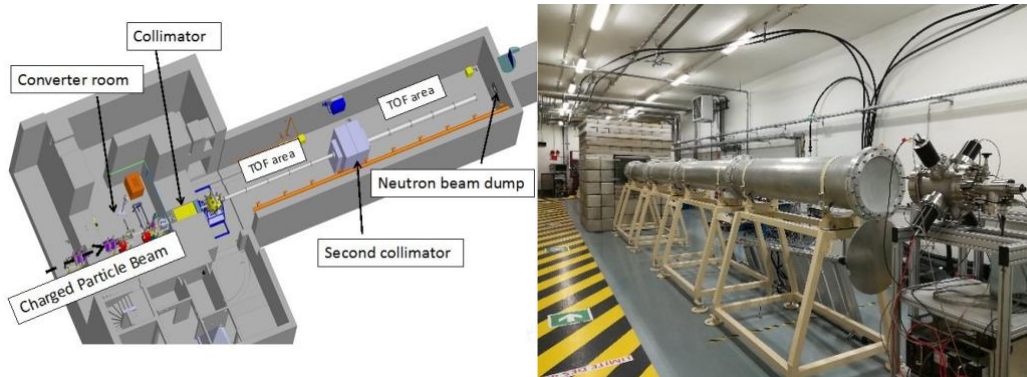


Figure 3 – Sketch of the neutron beam line at NFS (left part) and photo of our setup installed between the end of the second collimator and the beam dump (right part)

A new measurement of the cross-section of the  $^{19}\text{F}(n,\alpha)^{16}\text{N}$  reaction between the threshold energy and 40 MeV was performed with SCALP filled with pure  $\text{CF}_4$  at NFS in September 2021. The average deuteron intensity was set to  $7.5 \mu\text{A}$  to limit pile-up events in SCALP. The beam frequency was set to 730 kHz (chopper at 1/120) in order to avoid the overlap of two consecutive neutron bursts in the TOF area. The flight distance (the distance between the beryllium converter and the SCALP setup) was set at 28.431m to reach a high precision on the time of flight (Fig.3). Two neutron monitors on the NFS facility were available during this experiment: a micromegas and a liquid scintillator (LS monitor) respectively [4].

A second measurement was performed in October 2021 in order to measure (n,alpha) cross-section on oxygen 16. SCALP was then filled with a gas mixture made of  $\text{CF}_4$  (97%) and  $\text{CO}_2$  (3%). Characteristics of the neutron beam line were the same as the previous experiment. A fission chamber with an uranium 238 foil was added as a neutron monitor and installed at the entrance of the TOF area, just behind the first collimator.

### Data analysis

The first step in the analysis was to reconstruct the neutron time of flight from the time stamp  $t_{\text{PM}_i}$  given by each photomultiplier (i) and the time stamp  $t_{\text{HF}}$  given by the HF during neutron production by the facility. To determine the time of flight using the 4 PMTs, we calculated the light-weighted time of flight detected by the four photomultipliers. The time of flight is calculated as the difference between the weighted photomultipliers time and the HF time.

The time-of-flight distribution measured with SCALP shows that the gamma flash is very narrow. The time resolution of the gamma flash, which corresponds to the time-of-flight resolution measured by SCALP was found to be 1.3 ns ( $1\sigma$ ).

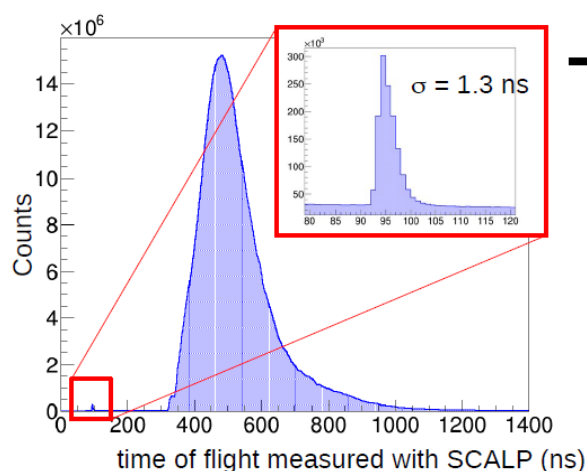


Figure 4 – Time of flight of incident particles (neutron and gamma). The loop shows the pic associated to prompt gamma ray

The kinetic energy of the incident neutrons detected by SCALP is calculated using the time of flight measured by the photomultipliers and the flight distance  $d = 28.413\text{m}$ . The spectrum ranges from 1 to 40 MeV, with a peak around 15 MeV. The neutron energy resolution is 0.4% at 10 MeV and remains below one percent between 0 and 40 MeV (Fig.5).

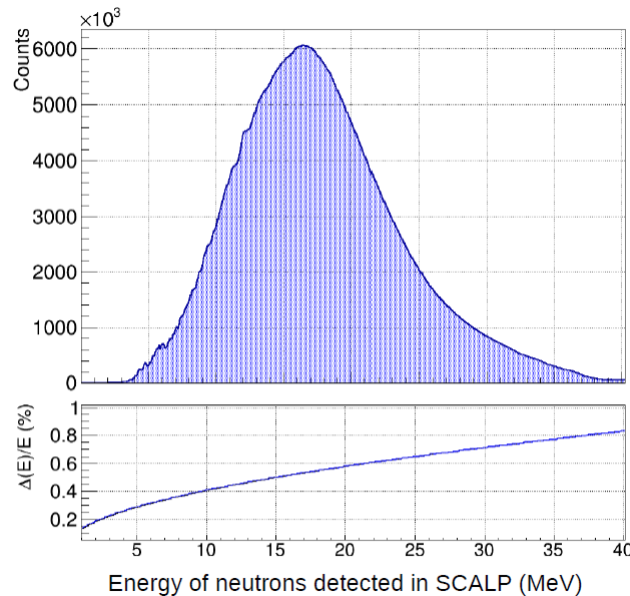


Figure 5 – Energy spectrum of the neutron detected with SCALP (upper side) and relative energy resolution as a function of the neutron energy (lower side)

### Reaction identification

The reconstruction of the incident neutron kinetic energy  $T_n$  associated with the measurement of the energy deposited in the ionization chamber  $E_{dep}$  allows one to construct an identification matrix for 2-body reactions in the chamber. Indeed, in that case, the difference between  $E_{dep}$  and  $T_n$  is simply equal to the Q-value of the reaction. Thus events belonging to a given reaction are expected to follow a straight line in the according  $(T_n, E_{dep})$  matrix and each of these two-body reactions can be identified by its Q-value.

| Reactions                              | Q (MeV) | $T_n$ threshold (MeV) |
|--|---------|-----------------------|
| $^{19}\text{F}(n,\alpha)^{16}\text{N}$ | -1.52   | 1.61                  |
| $^{19}\text{F}(n,p)^{19}\text{O}$      | -4.04   | 4.25                  |
| $^{19}\text{F}(n,d)^{18}\text{O}$      | -5.76   | 6.08                  |
| $^{12}\text{C}(n,\alpha)^9\text{Be}$   | -5.70   | 6.18                  |
| $^{19}\text{F}(n,t)^{17}\text{O}$      | -7.56   | 7.96                  |

Table 1 – Q-values for different reactions induced by neutron with fluorine 19 or carbon 13

With SCALP filled with pure  $\text{CF}_4$ , the  $^{19}\text{F}(n,\alpha)^{16}\text{N}$  reaction owns the highest Q reaction value that is well separated from the other reactions allowing the identification of the events associated to this reaction without ambiguities (Tab.1). The same applies to the reaction  $^{19}\text{F}(n,p)^{19}\text{O}$ . On the opposite, the  $^{12}\text{C}(n,\alpha)^9\text{Be}$  and  $^{19}\text{F}(n,d)^{18}\text{O}$  reactions carry Q values of -5.70 MeV and -5.76 MeV respectively (Tab.1) too close regarding the resolution of the SCALP ionization chamber, making it impossible to dissociate these two reactions. The ionization chamber is calibrated using the line  $^{12}\text{C}(n,\alpha)^9\text{Be}$ .

When plotting the deposited energy as function of the incident neutron energy (Fig.6), straight lines corresponding to two-body reactions identified by their Q values can be observed. However, it carries a lot of noise corresponding to three-body reactions, elastic and inelastic collisions. The  $^{19}\text{F}(n,\alpha)^{16}\text{N}$  and  $^{19}\text{F}(n,p)^{19}\text{O}$  reactions are identified and well separated from other reactions and parasitic reactions, enabling to measure their cross sections with the SCALP detector.

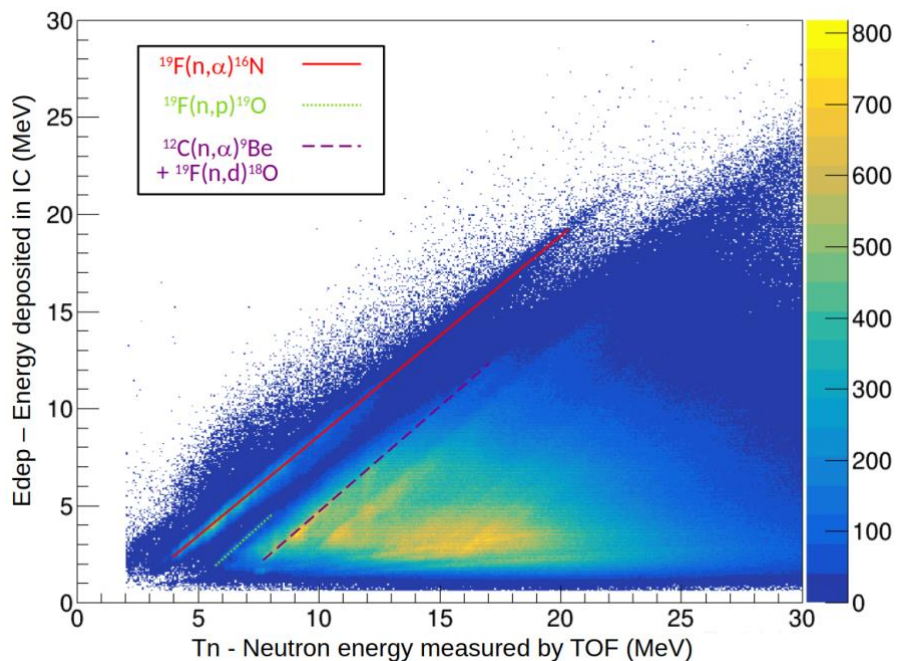


Figure 6 - The above identification matrix corresponds to the deposited energy  $E_{dep}$  in the ionization chamber as a function of the neutron kinetic energy  $T_n$  with the number of events shown in color in z-axis. Straight lines are observed, each of which corresponds to a reaction and can be identified by its Q-value.

#### Preliminary comparison with some previous works

The results of the SCALP experiment devoted to the  $^{19}\text{F}(n,\alpha)^{16}\text{N}$  reaction are shown in the Fig 7, given the  $^{19}\text{F}(n,\alpha)^{16}\text{N}$  events in the identification matrix. The number of counts per energy bin was corrected using the neutron flux distribution (thanks to the neutron monitors) and the detector response (thanks to GEANT4 simulations). Error bars include only statistical errors. In any case, one can see that some of the structures appearing in our data correspond to some previously observed. At around 8 MeV, SCALP measurements show contributions validated by the latest evaluations (JENDL-5) that were not observed in earlier evaluations (JEFF-3.3, ENDF/B-VIII.0). Between 9 MeV and 13.5 MeV, no measurements have been made before, so SCALP is likely to be the first cross section data set for the  $^{19}\text{F}(n,\alpha)^{16}\text{N}$  reaction in this energy range.

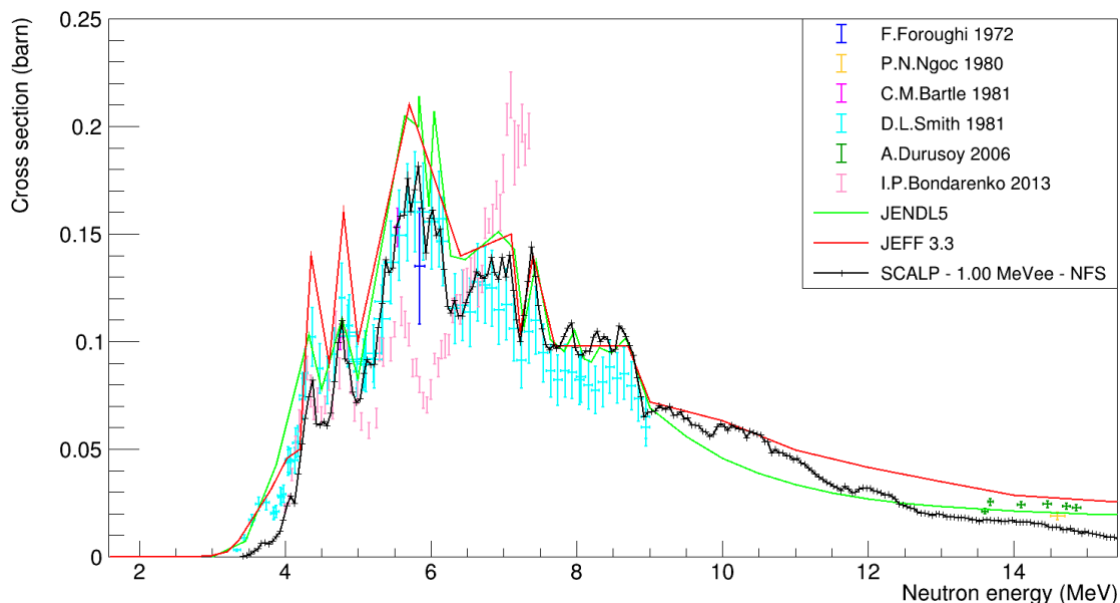


Figure 7 -  $^{19}\text{F}(n,\alpha)^{16}\text{N}$  reaction: cross-section (in barn) as a function of neutron energy (MeV). SCALP data (black dots, with only statistical uncertainties considered) vs some experimental data (colored dots) and evaluated data (lines) are shown.

### Problems encountered during these experiments

Two major problems were encountered during the experiments performed at NFS.

The first one is associated to a huge contamination (an illustration of this contamination is shown on fig.8 when using the nELBE neutron beam facility) that can be observed when plotting the deposited energy versus the drift time in the ionisation chamber. This contamination was also observed using the nELBE facility (Dresden, Germany) or an Am-Be source in our lab. This imply that this contamination is directly associated with some of the materials we are using in our detector.

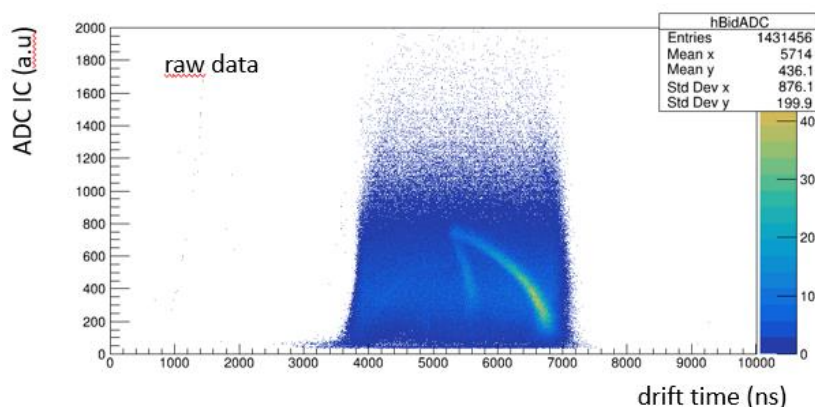


Figure 8 – Energy deposited (ADC IC) vs drift time in the ionisation chamber during a measurement at the nELBE facility. Two bananas are visible in the region above 5000 ns and correspond to neutron interaction with the hydrogen contained in the epoxy in one of the electrodes.

GEANT4 simulations were carried out to understand the origin of this contamination. We found that there are associated with the hydrogen contained in the epoxy in one of the electrodes. Modification of our setup are underway in order to remove completely this hydrogen.

The second problem we encountered is associated with the neutron monitors. The LS monitor is a thick liquid scintillator with a total efficiency of roughly 80%. This mean that it is not transparent to neutron. LS monitor was then installed between the second collimator and the SCALP detector during specific measurements. As the micromegas is always installed in the beam line at the entrance of the TOF area (thanks to its transparency to neutrons) we were able to determine neutron flux from the specific measurements and to include those neutron flux in our correction thanks to micromegas.

To determine neutron flux from LS monitor one has to know its efficiency vs neutron energy. Up to now, no measurements of this curve are available and one have to take into account simulation of it. However, it was found that the neutron flux derive from LS monitor was not in agreement with measurement performed with the fission chamber used as neutron monitor at NFS during our second experiment, discrepancies in form and amplitude were found. This can be due to the efficiency curve of the LS monitor and/or correction that have to be taken into account when transposing the results of the LS monitor at its position (behind the second collimator) to where was installed the fission chamber (at the entrance of the TOF area).

### Experimental program and Future works

The huge contamination observed in our data in all measurements are prohibitive for the study of (n,alpha) reactions on oxygen 16 as it implies rejection of two third of the statistics. On fluorine 19, this rejection lets us with enough statistics and we were able to provide new measurement of this reaction from the experiment performed at NFS. Same results will be

soon available from the same experiment performed at the nELBE facility. However, for the NFS measurements, the normalization procedure is fraught with error, given the monitors present during the experiment.

For this reason, we plan to make a new measurement of those (n,α) reactions at NFS taking advantage firstly of the improvement of our setup, secondly of the several neutron monitors now available on the NFS neutron beam line (not only the fission chamber but also the MoNHαP setup which is based on (n,p) reaction and silicon telescopes). In that sense we will be submitting a request for beam time at the next PAC at GANIL in October 2024.

## Conclusions

Some (n,α) reaction cross sections of interest for nuclear reactors exhibit large uncertainties. This is why new measurements of the cross section of (n,α) reactions was recommended. To respond to this request, LPC Caen has designed a new detector to measure (n,α) cross sections with a continuous neutron energy beam using the well-known time-of-flight technique. The very first experiment with this detector was carried out at SPIRAL2 - NFS (Caen, France).

The analysis of this new measurement is still on going. However results have shown that the  $^{19}\text{F}(n,\alpha)^{16}\text{N}$  of interest is well separated from the other reactions. To date, for the reaction  $^{19}\text{F}(n,\alpha)^{16}\text{N}$  one sees that some of the structures observed in the SCALP data are also reported in previous works, in addition new structures are observed and some structures are in agreement with the most recent evaluations.

Due to problems encountered with our setup, measurement of (n,α) reactions on oxygen 16 was not successful mainly because we have to remove two third of the statistics which is prohibitive for this measurement considering the beam time we had. In order to provide new measurement of this reaction in the coming years, we are upgrading our setup in order to solve the encountered problems and we will submit new proposals at the PAC meeting in GANIL before the end of this year.

## Bibliography

- [1] HPRL website at the NEA/OECD (Paris) <https://www.oecd-nea.org/dbdata/hprl/>
- [2] Sigfrid Stjernholm, Nuclear Data Uncertainty Quantification for Reactor Physics Parameters in Fluorine-19 based Molten Salt Reactors (WONDER-2023, Aix-en-Provence France, 2023)
- [3] G. Lehaut, SCALP: a detector for (n,α) cross-section measurements (ANIMA-2019)
- [4] <https://www.ganil-spiral2.eu/scientists/ganil-spiral-2-facilities/experimentalareas/nfs/>

## II. Neutron-induced light charged particle production at NFS, GANIL

Document prepared by D. Tarrío (UU), L. de Arruda (GANIL, UU), S. Pomp (UU).

As part of Task 2.1.2 an experiment to study  $^{nat}\text{C}(n, \text{lchp})$  reactions has been performed at the Neutrons For Science facility (NFS) at GANIL. The aim of the experiment, the first of its kind using the present setup at a white neutron beam, and one of the first experiments done at the NFS facility, is two-fold: From one side, to provide high quality nuclear data for this reaction, and from the other, to pave the way to future studies of the same type of reactions on other nuclei by developing the experimental setup and the analysis methods.

### Summary

This work intends to provide with accurate measurements on double-differential cross sections (DDX), with respect to emission angle and energy, for neutron-induced light-ion production in a carbon target. The white neutron beam from the Neutrons For Science (NFS) facility at GANIL has been used, covering a range from about 1 MeV up to 40 MeV. The experimental setup Medley is based on an existing older version which was originally intended to be used at quasi-monoenergetic neutron beams only. Along this project, the setup has been upgraded to be used at white neutron beams, and the detection capabilities have been improved, making it suitable for further experimental campaigns, as shown by the latest experiments on Fe and Cr performed in 2023. The experiment on carbon, done in October 2022, was one of the first experiments done at the NFS facility. The data analysis is still ongoing, and the main achievements as well as the status of the analysis are reported here.

### Experimental setup

The experimental setup Medley (Figs. 1 and 2) has been developed at Uppsala University and earlier used at the former neutron facility TSL in Uppsala, with quasi-monoenergetic neutron beams [Pom10, Jan15]. Medley is designed for the detection of charged particles over a wide dynamic range. It consists of eight three-element telescopes mounted inside a vacuum chamber with inner diameter of 800 mm. The telescopes are placed at  $20^\circ$  intervals, covering emission angles from  $20^\circ$  to  $160^\circ$  simultaneously (see Fig. 2), and mounted onto a rotatable plate, thus allowing us to measure at any emission angle.

In 2019, the Medley setup was moved definitely from Uppsala to GANIL-NFS (Fig. 1). Since then, it has been used in different beam tests as well as for official campaigns, being the measurement reported here the first physics experiment done with Medley at NFS, and also one of the very first experiments done at the white neutron beam of NFS.

Each telescope consists of two fully depleted  $\Delta E$  silicon surface barrier detectors (SSBD) and a CsI(Tl) crystal. The thicknesses of the first eight  $\Delta E$  detectors ( $\Delta E1$ ) range between 20 and 60  $\mu\text{m}$ . For the second SSBD ( $\Delta E2$ ) the thicknesses range between 400 and 1000  $\mu\text{m}$ . The SSBD are all 23.9 mm in diameter (nominal). The CsI(Tl) crystals have 50 mm in length and 40 mm in diameter, and are able to fully stop the detected particles. Each crystal is connected to a read-out photodiode. Most of the telescopes were, typically, placed at a distance of 15 cm from the target, covering a solid angle of about 20 msr. By using the energy deposited in the different detectors ( $\Delta E$ - $\Delta E$ -E technique), it is possible to identify the different light ions.

In order to be able to perform experiments at a white neutron beam, as the one provided at NFS, the setup has been upgraded to incorporate time-of-flight capabilities in the detectors. For that, new readout preamplifiers have been developed in close collaboration with GANIL.



Figure 1: The Medley setup installed at NFS, just after the exit of the collimator.

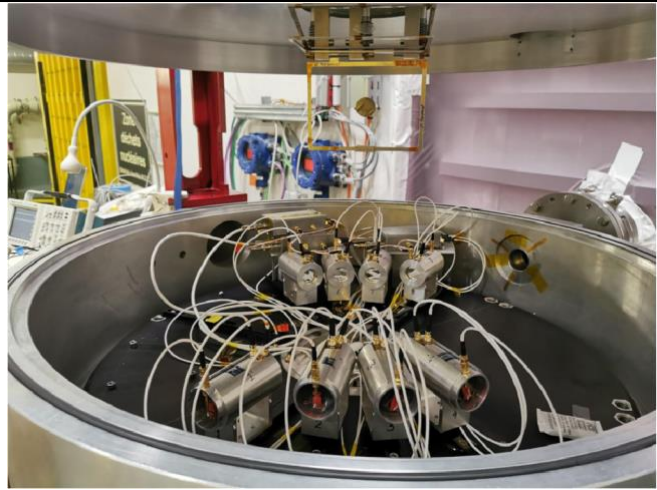


Figure 2: Inner view of the Medley chamber during the 2022 campaign. The eight telescopes are pointing to the central part of the chamber. The circular carbon target can be seen in the upper side, attached to the lid.

## Targets

In this experiment, circular targets of 25 mm in diameter have been used: one natural carbon target of 75- $\mu\text{m}$  thick, and one plastic  $\text{CH}_2$  target of 50- $\mu\text{m}$ , which is needed to measure the neutron flux using the known cross-section of the neutron-proton elastic scattering from H. Each target is attached to an aluminum rectangular frame using tungsten wires of 25  $\mu\text{m}$  in thickness (see Fig. 3). The Medley setup can hold three targets inside, being possible to change the one which is exposed to the neutron beam without opening the chamber.

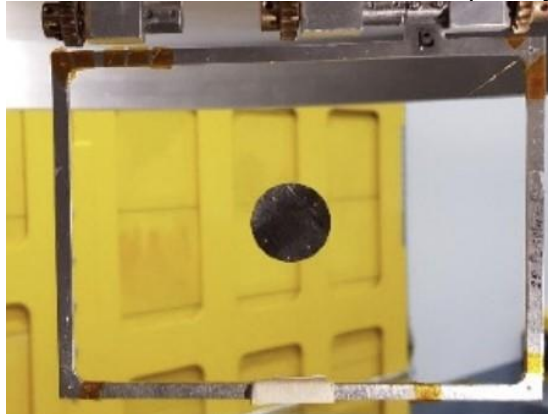


Figure 3: The carbon target, held in an aluminum frame in the Medley chamber using 25- $\mu\text{m}$  thick tungsten wires attached to the corners of the frame (practically invisible in the photo).

## Experimental campaign

The proposal for this experiment was approved by the GANIL Program Advisory Committee in 2020 [Pro20]. This experiment was initially planned for being done in year 2021. However, because of a problem with the neutron converter of NFS, the beam time was canceled soon after the start of the experiment. So, this experiment has been finally done in October 2022.

## Signal processing

All the 24 detectors were connected to charge preamplifiers developed by the electronics group of GANIL and installed outside the vacuum chamber, except for those connected to the 50- $\mu\text{m}$  Silicon detectors, which were installed inside the vacuum chamber to minimize the electronic noise. All the preamplified signals were read by a digital acquisition module NUMEXO2 (developed at GANIL), which performs an online signal processing by software: a trapezoidal filter is used to determine the amplitude signal; for the signals of the second silicon in each telescope, the time stamp is also determined using a digital constant filter discriminator. These variables are then stored to disk for online and offline analysis.

## Calibration of deposited energy

The first and second silicon detectors in each telescope have been calibrated, after the experiment, using the reference peaks of a triple alpha source ( $^{239}\text{Pu}$ ,  $^{241}\text{Am}$  and  $^{244}\text{Cm}$ ). Moreover, the punchthrough energies of the different types of detected light-ions detected (p, d, t) when passing the different detectors, and given by SRIM [Zie10] and KaliVeda [Kal] simulations, have been also used for the calibrations.

## Particle identification

By plotting the energy loss in each of the three elements of the telescope, it is possible to identify the different light-ions produced. Figure 4 shows an example, using a small subset of statistics, of the correlation found between the energy deposited in the first silicon  $\Delta E_1$ , in the second silicon  $\Delta E_2$  (left figure) and between  $\Delta E_2$  and the energy deposited in the scintillator  $\Delta E_3$  (right figure) for the telescope placed at  $20^\circ$ . The good energy resolution of the setup allows to distinguish between the different light-ions (p, d, t,  $^3\text{He}$ ,  $\alpha$ ) produced in the C target.

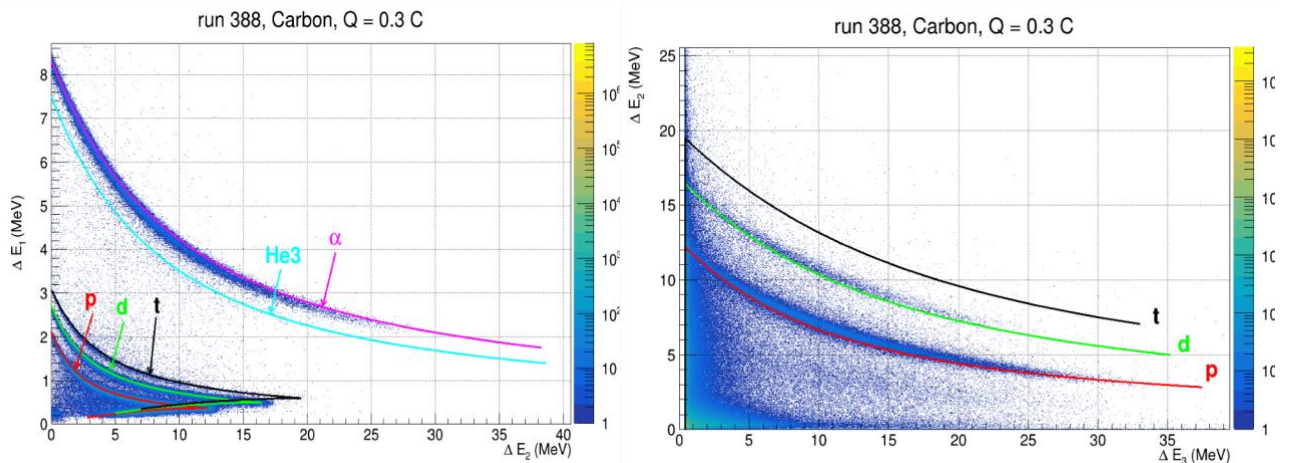


Figure 4: Energy deposited by the light-ions emitted by the C target in the telescope placed at  $20^\circ$ . Left: Energy deposited in the first silicon ( $\Delta E_1$ ) vs. energy in the second silicon ( $\Delta E_2$ ). Right: Only those ions having enough energy to pass through the second silicon are able to deposit energy in the CsI crystal, and they appear as bands when plotting the energy deposited in the second silicon ( $\Delta E_2$ ) vs. energy deposited in the CsI ( $\Delta E_3$ ). The continuous lines are from simulations with KaliVeda.

## Neutron energy measurement

The energy of the neutron that induces a particular reaction is measured by its time of flight, as schematically illustrated in Fig. 5. The detection of a light-ion in one of the telescopes sets a “start” for the time-of-flight, and the next pulse of the linear accelerator is used as the “stop”. The time determined in this way includes also the time required by the ion to travel from the C target to the telescope. The latter time can be determined using the kinetic energy of the ion (measured from the total deposited energy in the telescope), and its mass, which is known

thanks to the identification performed in the telescope. The arrival time of the  $\gamma$ -flash at the detectors is used as the time origin reference for time measurements.

All the light-ion production reactions in  $^{12}\text{C}$  are threshold reactions; among them, the  $(n,\alpha)$  reactions are the ones having the lowest threshold, that corresponds to a neutron energy of  $\sim 7$  MeV. For neutrons with that energy, it takes 150 ns to travel from the neutron converter to the Medley target. This is a much shorter time than the beam repetition period of 1.1  $\mu\text{s}$ . In consequence, there is no overlap between reactions produced by neutrons from different beam pulses.

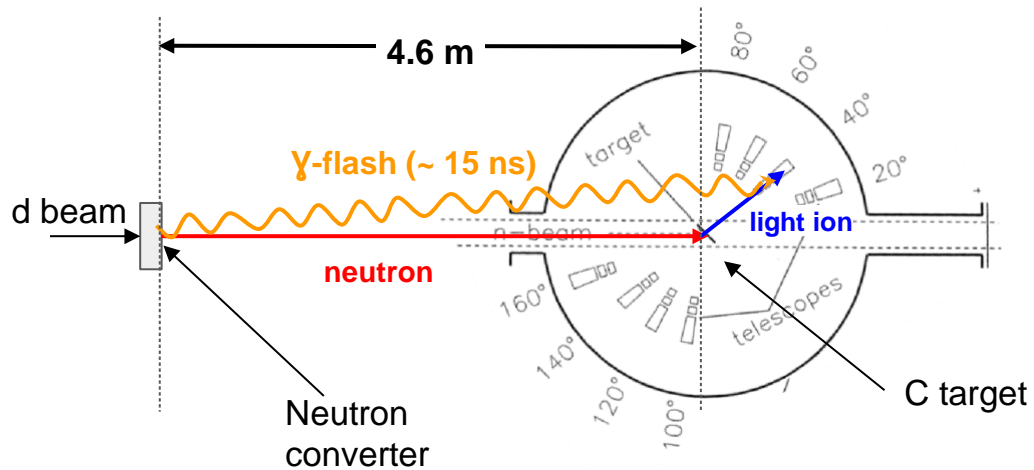


Figure 5: Principle of the neutron energy measurement using the time-of-flight technique. See text for details.

### Time-of-flight to energy calibration and open issues

The absolute cross-sections will be determined from the measured data by comparison to the number of protons being elastically scattered by neutrons in a  $\text{CH}_2$  target.

As mentioned earlier, the use of a hydrogen-rich target, such as  $\text{CH}_2$ , allows us to deduce the spectral neutron flux from the neutron-proton elastically scattered events. In this case, the energy of the scattered proton is determined by the incident neutron energy, and by the emission angle. In this way, it will be possible to deduce absolute cross-sections for light-ion production in carbon from this experiment.

When looking at the time-energy correlations, it was found that there is a shift in the time-of-flight depending on whether the detected particle has (or not) enough energy to pass through the second silicon. Fig. 6 (left) shows the total energy deposited in the telescope by elastically scattered protons versus the neutron energy calculated from the time of flight. Instead of the expected linear dependence (red line), a deviation is observed at energies starting around the punch through energy of the second silicon (13 MeV for protons, approximately). This unexpected behavior is being investigated. Up to now, it seems that the origin is a malfunction of the digital constant-fraction discriminator that determines, from the second silicon detector, the time instant at which the particle enters the detector (in this case, a proton). This issue also affects deuterons and tritons, whereas alphas are not affected because they are always stopped at the second Silicon detector.

A potential solution to this problem has been developed: a correction factor has been calculated to modify the measured time-of-flight depending on the energy deposited on the telescope, to match the expected time-of-flight corresponding to the proton energy. Figure 7 shows that correction factor obtained for protons for three different telescopes, placed at  $20^\circ$ ,

40° and 60° with respect to the beam line. Similar factors for deuterons and tritons have been determined, but omitted from this report. Helium isotopes are stopped in the second silicon and do not need such a correction either.

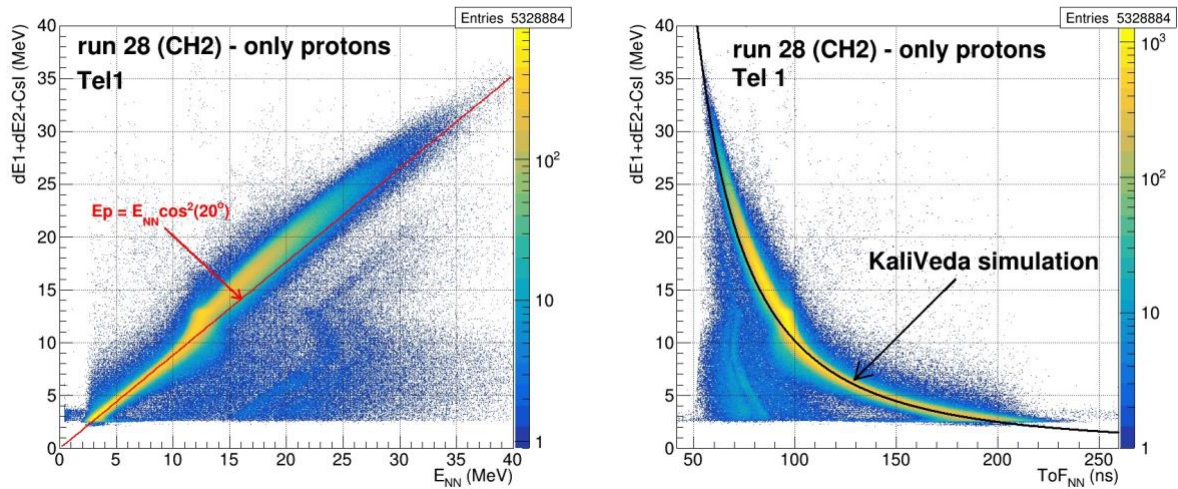


Figure 6: Experimental values of the kinetic energies of the outgoing protons from elastic collisions with neutrons, plotted as a function of neutron energy (left) and as a function of neutron time-of-flight (right). The experimental data deviate from the theoretical behavior (solid lines) for energies above the punch-through energy of the second silicon detector in the telescope, which is about 13 MeV in this particular case.

corrections for protons, runs 370+ 407 (CH<sub>2</sub>)

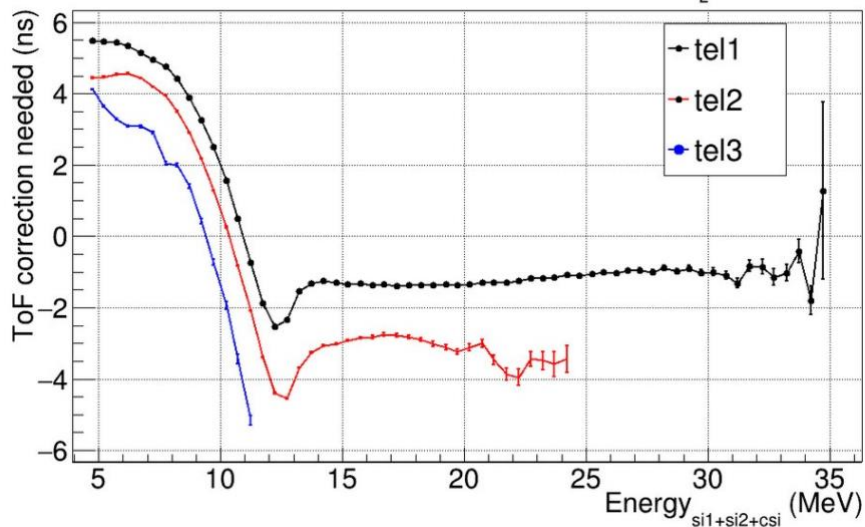


Figure 7: Time-of-flight correction for protons deduced from the measurement of the energy deposited by elastically scattered protons by neutrons in the CH<sub>2</sub> target. The different curves correspond to the telescopes placed at 20°, 40° and 60° with respect to the beam line.

### Neutron flux determination

To obtain absolute measurements on the cross sections, the neutron flux must be determined independently. To do that, a CH<sub>2</sub> target has been also exposed to the neutron beam. By measuring the number of scattered protons at 20°, and using the differential cross-section of neutron-proton elastic scattering at the same angle, provided by ENDF/B-VI evaluation, it is possible to determine the neutron flux, as shown in Fig. 8. The blue histogram has been obtained from the raw data, which leads to an unphysical peak at energies around 13 MeV

caused by punchthrough of protons through the second silicon, explained in the previous section. After using the correction from Fig. 6, the red histogram is obtained, in which this effect has been largely suppressed, reaching a better agreement with the flux shown by the black line. This black line corresponds to a flux measurement based on fission of  $^{238}\text{U}$  using a PPAC chamber. Still, this correction method is being improving with the aim of eliminating completely that unphysical peak. Nevertheless, the principle of operation is working and the use of a more detailed parametrization of the correction factor, with specific coefficients for each individual telescope, should solve the issue.

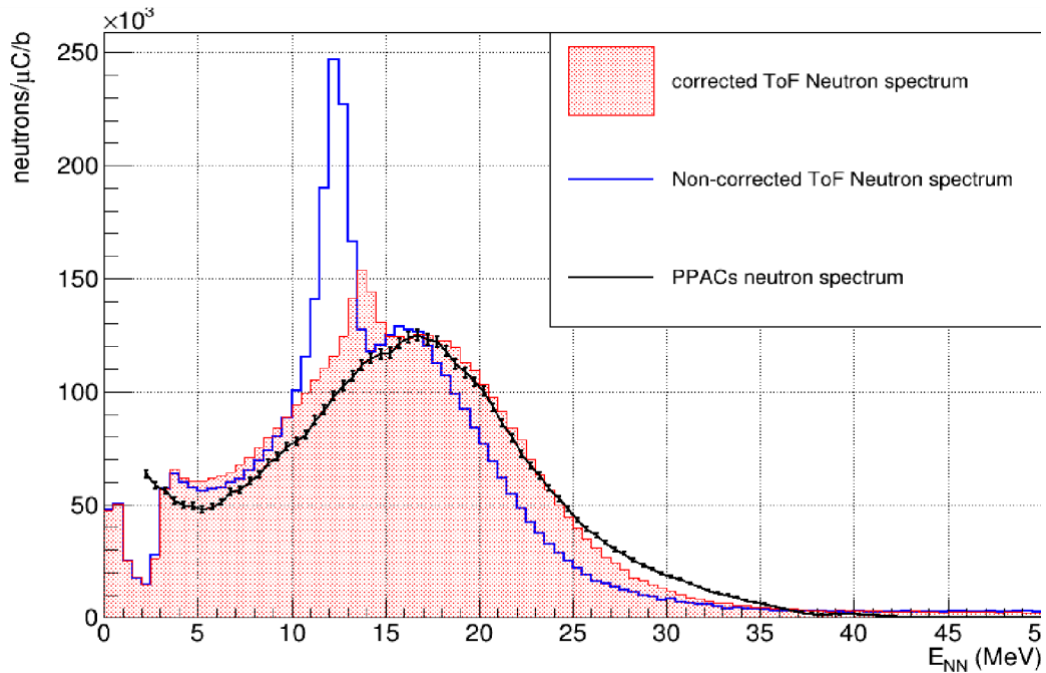
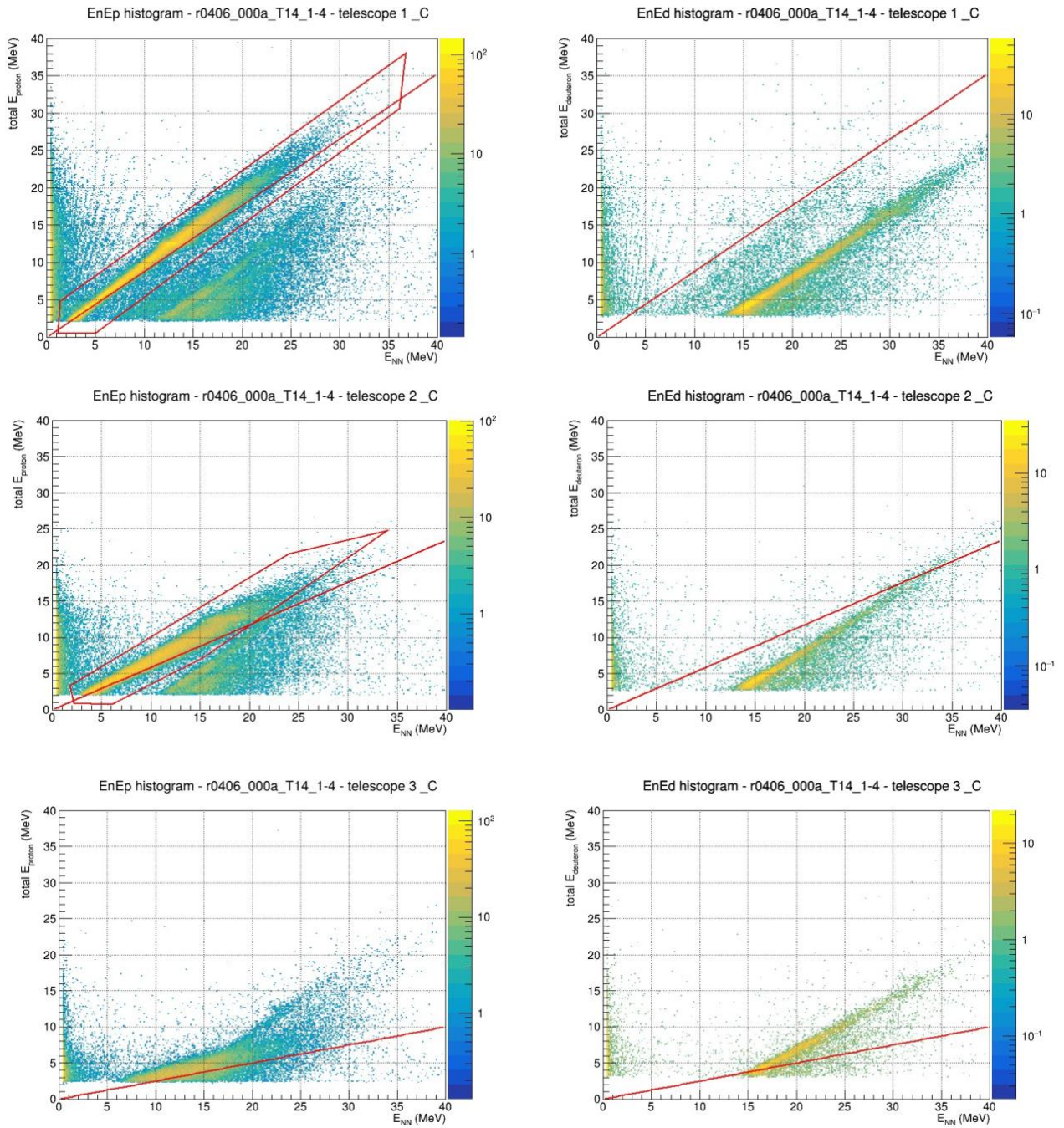


Figure 8: Neutron spectrum deduced from neutron-proton elastic scattering on  $\text{CH}_2$ . The blue and red histograms represent the results before and after the time-of-flight correction to the data, determined from Fig. 6. The black line is the neutron flux measured by an independent neutron beam monitor based on PPACs.

### **Energy and angular distributions of emitted ions**

By selecting each ion, according to the plots shown in Fig. 4, it is possible to study the energy distribution of the emitted ion as a function of the neutron energy. Fig. 9 shows the energy of protons (plots on the left column) and of the deuterons (plots on the right column) as a function of neutron energy. Each of the rows corresponds to one telescope: placed at 20, 40 and 60 degrees, respectively. It must be noted that in this experiment we can only study inclusive reactions, that is, the summed contribution of all reaction channels where a certain type of light-ion is produced.



*Figure 9: Energy of emitted protons (left column) and of emitted deuterons (right column) as a function of the incoming neutron energy. Each of the rows corresponds to one different telescope: at 20, 40 and 60 degrees, respectively. The red lines indicate the energy corresponding to elastically scattered protons. A large background of elastically scattered protons in the C target (which should not exist) is observed at all angles. For 20 and 40 degrees, it can be easily discriminated from the protons emitted in neutron-induced reactions in C and they are removed from the analysis by omitting the events within the red contours.*

The most striking feature of the plots on the left column (corresponding to proton emission) is the existence of a band of protons with energies corresponding to those of elastically scattered by neutrons from the beam, which theoretical value is indicated by the red straight line in all the plots. This characteristic indicates a possible contamination of hydrogen in the

C sample. Most likely of water molecules attached to the interstices of the graphite lattice. In any case, as seen in Fig. 9, those events can be, for telescopes at  $20^\circ$  and  $40^\circ$ , easily discriminated from protons emitted in neutron-reactions with carbon by applying a graphical cut to the data. Regarding the telescope at  $60^\circ$ , there is an overlap between the elastic scattering band and the protons emitted from carbon, so that a background subtraction must be done by estimating the number of expected events in the scattering band from a comparison to the other angles. For the telescope at  $80^\circ$ , the energies of the scattered protons are below the detection level and, therefore, the graph is not included.

The diagonal bands in the upper-left plot below the elastic scattering band show clearly the opening of several channels at about 10 and 12 MeV neutron energy, showing also the capability of this setup to study individual reaction channels.

By doing a selection in the neutron energy calculated from the time-of-flight, it is possible to obtain the energy distribution of the emitted ions (measured as total deposited energy in a telescope), for each angle defined by the position of the telescopes, and for each neutron energy. That is, we can deduce directly the double-differential cross-sections for production of each light-ion, as a function of neutron energy.

Moreover, by integrating over one or two of these variables (ion energy and emission angle), it is possible to deduce the single-differential and the total production cross-sections for each light-ion, as a function of neutron energy.

Figure 10 shows an example of the angular distribution of protons (left) and deuterons (right) emitted from the C target, for different neutron energies. The corrections due to the energy losses of the particles in the targets have not been applied yet. The results show clearly how the distribution of emitted particles tends to be more forward-peaked for higher energies of the incoming neutron.

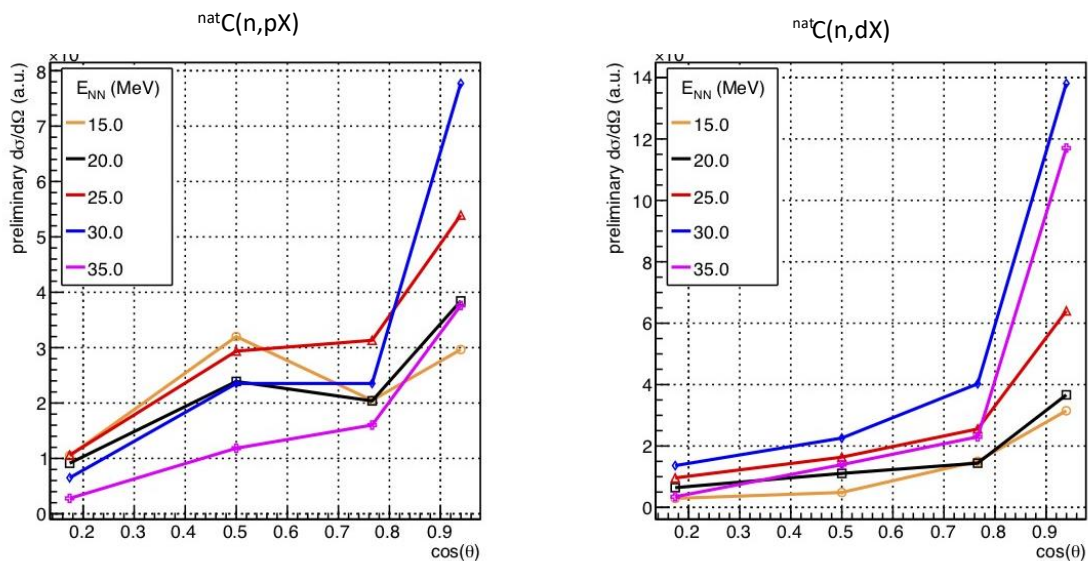


Figure 10: Angular distributions of protons (left) and deuterons (right) emitted from the  $^{nat}\text{C}$  target, for different neutron energies indicated in the legend. Energy losses of the particles in the target are not taken into account yet.

Alternatively, Figure 11 shows the values of the total production of protons (left) and deuterons (right) for each of the four forward telescopes ( $20^\circ$ ,  $40^\circ$ ,  $60^\circ$  and  $80^\circ$ ), as a function of the neutron energy. To obtain those values, the neutron flux shown in Fig. 8 has been used. Therefore, since the value of the flux is affected by the non-physical peak already mentioned before, the results shown in Figure 11 are rather qualitative. However, they are useful to show the type of results that the analysis will produce when finalized, covering from about 4 MeV

neutron energy, up to 40 MeV. The peak observed at 10 MeV observed for protons emitted at 60° (left plot) is a consequence of an incomplete discrimination of the scattered protons from Fig. 9. That will be improved in next steps of the analysis.

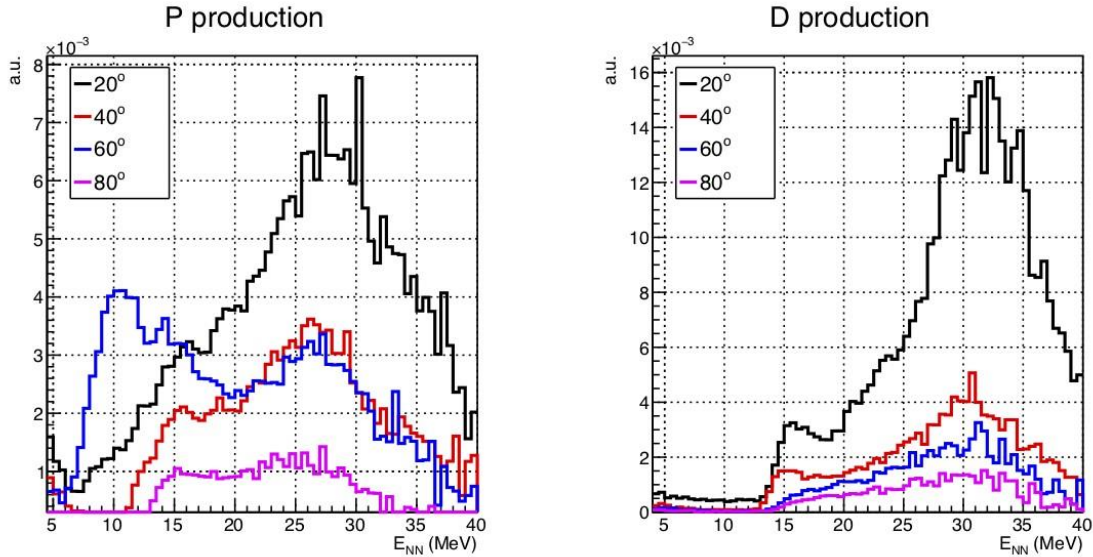


Figure 11: Production cross-section of protons (left) and deuterons (right) for  $^{nat}\text{C}$ , as a function of the neutron energy, and for each of the angular directions defined by the position of the forward telescopes. Energy losses of the particles in the target are not taken into account yet. The peak at 10 MeV for protons emitted at 60° (left plot) is a consequence of an incomplete discrimination of the scattered protons from Fig. 9.

### Summary

An experiment devoted to the measurement of cross-sections of  $^{nat}\text{C}(n, \text{lchp})$ , has been done at GANIL-NFS in October 2022. This was the first experiment with the Medley setup at a white neutron beam, and also one of the first experiments done at the NFS facility.

The analysis of the experiment, as well as the development of the analysis routines, is part of a Ph.D. thesis started at the end of 2022, and it is still ongoing.

The good performance exhibited by the setup has made possible to identify individual isotopes of H (p, d, t) and He ( $^3\text{He}$ ,  $\alpha$ ) produced in neutron-induced reactions. Moreover, it has been possible to determine the neutron energy of each individual event with a resolution well below than 1 MeV, which will allow for determination of double-differential cross-sections as a function of the neutron energy.

However, unexpected challenges, as the observed dependence of the time-of-flight with the particle energy, makes the analysis more complex than anticipated. In any case, the dependences of the physical quantities and the relations between the data observed with different telescopes correspond to the expected situation, and a correction factor has been developed to correct for those issues.

As a consequence, the results included here show the capabilities of the setup in discriminating between individual light ions, and on providing data on cross-sections with respect to emission angle and to emitted ion energy, as a function of neutron energies in a wide neutron energy range, which spans from about 4 MeV up to 40 MeV.

Corrections for energy losses of the ions within the target are still pending to be included. A method for those corrections has been developed and successfully applied in the past to similar experiments with quasi-monoenergetic neutron beams [Pom10] so that it is expected to be used in this new experiment with minor variations.

Therefore, it is expected that the completion of the data analysis will provide with accurate nuclear data on the double-differential cross-sections of production of light-ions in carbon in a wide neutron energy range. Moreover, this experiment paves the way to study other nuclei. In fact, studies on Cr and Fe targets have been recently done in November 2023. Those data are also being analyzed

## **References**

- [Jan15] K. Jansson et al., "Designing an upgrade of the Medley setup for light-ion and fission cross-section measurements", Nucl. Inst. Meth. Phys. Res. A 794, 141 (2015). <https://doi.org/10.1016/j.nima.2015.05.001>
- [Kal] <http://indra.in2p3.fr/kaliveda/>
- [Pom07] S. Pomp and U. Tippawan, "An iterative procedure to obtain inverse response functions for thick-target correction of measured charged-particle spectra", Nucl. Inst. Meth. Phys. Res. A 572, 893 (2007). <https://doi.org/10.1016/j.nima.2006.11.058>
- [Pom10] S. Pomp et al., "A Medley with over ten years of (mostly) light-ion production measurements at The Svedberg Laboratory", EPJ Web of Conferences 8, 07013 (2010). <https://doi.org/10.1051/epjconf/20100807013>
- [Pro20] A. Prokofiev et al., "LIONS - Light-Ion Production Studies with Medley at the NFS facility", Proposal E800\_20, submitted to GANIL PAC in May 2020.
- [Led14] X. Ledoux et al., "The Neutrons for Science Facility at SPIRAL-2", Nucl. Data Sheets 119, 353 (2014). <https://doi.org/10.1016/j.nds.2014.08.097>
- [Led17] X. Ledoux et al., "The neutrons for science facility at SPIRAL-2", EPJ Web Conf. 146, 03003 (2017). <https://doi.org/10.1051/epjconf/201714603003>
- [Zie10] J. F. Ziegler et al., "SRIM – The stopping and range of ions in matter (2010)", Nucl. Inst. Meth. Phys. Res. B 268, 1818 (2010). <https://doi.org/10.1016/j.nimb.2010.02.091>